TECHNICAL MEMORANDUM

681

Understanding advances in the simulation of intraseasonal variability in the ECMWF model. Part I: The representation of the MJO

L. C. Hirons[1], P. Inness[1], F. Vitart[2], P. Bechtold[2]

Research Department

[1]Department of Meteorology, University of Reading, Earley Gate, PO Box 243, Reading, RG6 6BB
[2]ECMWF

To be submitted to Q. J. R. Meteorol. Soc

July 9, 2012

European Centre for Medium-Range Weather Forecasts
Europäisches Zentrum für mittelfristige Wettervorhersage
Centre européen pour les prévisions météorologiques à moyen terme

Series: ECMWF Technical Memoranda

A full list of ECMWF Publications can be found on our web site under:
http://www.ecmwf.int/publications/

Contact: library@ecmwf.int

European Centre for Medium-Range Weather Forecasts
Shinfield Park, Reading, RG2 9AX, England

Abstract

As a major mode of intraseasonal variability, which interacts with weather and climate systems on a near-global scale, the Madden-Julian Oscillation (MJO) is a crucial source of predictability for numerical weather prediction (NWP) models. Despite its global significance and comprehensive investigation, improvements in the representation of the MJO in an NWP context remain elusive. However, recent modifications to the model physics in Cycle 32r3 of the ECMWF model led to advances in the representation of atmospheric variability and the unprecedented propagation of the MJO signal through the entire integration period.

In light of these recent advances, a set of hindcast experiments have been designed to assess the sensitivity of MJO simulation to the formulation of convection. Through the application of established MJO diagnostics, it is shown that the improvements in the representation of the MJO can be directly attributed to the Cycle 32r3 convective parameterization. Furthermore, the improvements are attributed to the move from a moisture-convergent- to a relative-humidity-dependent formulation for organised deep entrainment. It is concluded that, in order to understand the physical mechanisms through which a relative-humidity-dependent formulation for entrainment led to an improved simulation of the MJO, a more process-based approach should be taken. The application of process-based diagnostics to the hindcast experiments presented here will be the focus of Part II of this study.

1 Introduction

The Madden-Julian Oscillation (MJO; Madden and Julian, 1971) is the dominant mode of intraseasonal variability in the tropics. It can be characterised as a planetary-scale convective anomaly with an associated overturning atmospheric circulation which propagates east from the Indian Ocean through the Maritime Continent into the West Pacific. An MJO event lasts between 30 and 60 days, however, the phenomenon has been shown to be highly episodic (Salby *et al.*, 1994). For a detailed review of the structure and lifecycle of the MJO see Zhang (2005).

Modelling the MJO challenges our understanding of convective processes in the tropical atmosphere because it encompasses multi-scale interactions (Nakazawa, 1988), ranging from the triggering of individual convective plumes on sub-grid scales, to the organisation and propagation of convection on a planetary-scale. The MJO is an important source of predictability in its own right, but its interactions with other components of the climate system make it a necessary phenomenon for models to capture. The passage of the MJO through the equatorial Indo-Pacific has been shown to interact with the Asian (e.g. Lawrence and Webster, 2002) and Australian (e.g. Hendon and Liebmann, 1990) Summer Monsoon systems, as well as influence rainfall variability on a near-global scale (e.g. Bond and Vecchi, 2003; Matthews, 2004). Studies have also shown that the MJO modulates tropical cyclogenesis (e.g. Mo, 2000; Maloney and Hartmann, 2000) and can affect the strength and onset of the El Niño Southern Oscillation (ENSO; Kessler and McPhaden, 1995). Despite its global importance in the climate system and extensive study in recent decades, deficiencies remain in our ability to model the phenomenon (e.g. Slingo *et al.*, 1996; Lin *et al.*, 2006).

This study examines the representation of the MJO in the Integrated Forecasting System (IFS) at the European Centre for Medium-Range Weather Forecasting (ECMWF), a state-of-the-art numerical weather prediction (NWP) model. Previously, the IFS exhibited a distinct loss of MJO amplitude in the early days of the forecast and had difficulty propagating the convective signal through the Maritime Continent (Vitart, 2003), a problem common to other models (e.g. Inness and Slingo, 2006). However, skilful predictability of the MJO was improved through coupling the IFS to a mixed-layer ocean model (Woolnough *et al.*, 2007) and modifying the model physics (Vitart *et al.*, 2007).

Table 1: Summary of control IFS versions (Cy31r1 and OPER) and hindcast experiments (CONV, ENTRN and OPER). YOTC (Year of tropical convection) refers to a period, from May 2008 to January 2010, of targeted observations, modelling and forecasting activities coordinated by the World Climate and Weather Research Programs (WCRP and WWRP).

Control IFS Experiments	Integration period	Analysis	Resolution	Radiation	**Convection** τ, ε_{org}	Cycle
Cy31r1	YOTC period	ERA-Interim	T_L255L60	'old'	3600s, ε_{org}^{MC}	Cy31r1
OPER	YOTC period	Operational	T_L799L91	McRad	720-10800s, ε_{org}^{RH}	Cy32r3-Cy35r3
CONV	05/2008-07/2009	Operational	T_L799L91	McRad	720s, ε_{org}^{MC}	Cy33r1
ENTRN	05/2008-07/2009	Operational	T_L799L91	McRad	720-10800s, 0.5*ε_{org}^{RH}	Cy33r1
CAPE	05/2008-04/2009	Operational	T_L799L91	McRad	720s, ε_{org}^{RH}	Cy33r1

More recent modifications to the convection and vertical diffusion schemes in cycle 32r3 (Cy32r3) of the IFS led to significant advances in the simulation of atmospheric variability on intraseasonal timescales; Cy32r3 was the first version of the IFS that was able to realistically sustain the amplitude of the MJO throughout the integration period (Bechtold *et al.*, 2008; hereafter B08). The experiments carried out in this study (section 2.1), investigate which aspects of the Cy32r3 physics changes were responsible for the improved representation of the MJO in the IFS. The analysis techniques used for model evaluation are described in section 2.2. The attribution of advances in MJO simulation to particular aspects of the Cy32r3 convection scheme will be shown in section 3, discussion and conclusion will follow in sections 4 and 5 respectively. Understanding the physical mechanisms through which these advances in MJO simulation were achieved will be examined in Part II (Hirons *et al.*, 2012).

2 Methodology

2.1 Model description and experimental setup

The revisions to the convection scheme in Cy32r3 (B08) included (a) replacing the constant, resolution-dependent convective available potential energy (CAPE) adjustment timescale (τ) in the closure for deep convection with a variable τ, dependent on the updraught vertical velocity averaged over the cloud depth; and (b) changing the dependence of organised entrainment in the formulation for deep convection from a moisture-convergent-dependent formulation (ε_{org}^{MC}) to one dependent on the relative humidity of the surrounding environment (ε_{org}^{RH}). The motivation for the entrainment formulation change was twofold. First, changing the control on convection was aimed at removing known model errors. The previous ε_{org}^{MC} created a nonlinear feedback between convection and large-scale dynamics that resulted in errors in precipitation and cloud-top height (B08). Second, changing to ε_{org}^{RH} addressed the emerging recognition in the literature that convective parameterizations in NWP models do not exhibit sufficient sensitivity to environmental humidity (e.g. Redelsperger *et al.*, 2002; Derbyshire *et al.*, 2004).

To understand the effects of different aspects of the Cy32r3 convective parameterization a series of hindcast experiments, which differ only in their formulation of convection, have been performed during the Year of Tropical Convection (YOTC) period (Table 1). The hindcast experiments, initialised in May 2008, are compared to two control versions of the IFS (Cy31r1 and OPER). Cycle 31r1 (Cy31r1), a pre-Cy32r3 cycle of the IFS that was used to produce the ERA-Interim reanalysis dataset (Dee *et al.*, 2011). The atmospheric component of the model is run at T_L255 resolution (about 80 km) with 60 levels in the vertical, a model top at 0.1 hPa and model time step of 30 minutes. The integrations are initialised using ERA-Interim reanalysis and forced daily by persisted SSTs from the NCEP high-resolution, real-time, global (RTG) SST reanalysis until January 2009 and the National Centre for Ocean Forecasting (NCOF) Operational Sea Surface Temperature and Sea Ice Analysis (OSTIA) after January 2009. Cy31r1 uses the ÔoldÕ radiation scheme, before the introduction of the cycle 32r2 McRad scheme (Morcrette *et al.*, 2007). The convection scheme in Cy31r1 (prior to the modifications of B08) uses ε_{org}^{MC} and a constant, resolution-dependent τ (at T_L255, τ = 3600s).

OPER refers to the evolving operational IFS cycle during the YOTC period, from Cy32r3 to Cy35r3 (all including the B08 modifications). The atmospheric resolution is T_L799 (about 25 km) with 91 levels in the vertical, a model top at 0.01 hPa and model time step of 12 minutes. The integrations are initialised using the YOTC operational analysis and forced by persisted SST anomalies from NCEP RTG prior to October 2008 and from OSTIA after October 2008. The persisted SST anomalies are calculated by persisting the initial SST anomalies from the climatological seasonal cycle through the forecast, with the seasonal cycle continuing to evolve throughout the integration. The new McRad radiation scheme is used throughout OPER. The convection scheme in OPER uses ε_{org}^{RH} and a variable τ (at T_L799, $720 < \tau < 10800$s).

All the hindcast experiments (CONV, ENTRN and CAPE) were performed using Cycle 33r1 (Cy33r1), a post-Cy32r3 cycle including the McRad radiation scheme. The horizontal resolution and initialisation of the hindcast experiments is identical to OPER. CONV is a post-Cy32r3 cycle with a pre-Cy32r3 convection scheme, it uses ε_{org}^{MC} and a constant τ. The convection scheme in CAPE uses a constant τ and ε_{org}^{RH}. The convection scheme in ENTRN uses a variable τ and $0.5 * \varepsilon_{org}^{RH}$ (see Table 1 for a summary). Halving the relative-humidity-dependent term in the formulation for entrainment amounts to approximately a 25 % reduction in the overall entrainment. Table 2 indicates which individual convection modifications are highlighted by comparisons between versions of the IFS described in Table 1, for example comparing CAPE and CONV isolates the effect of the ε_{org}^{RH} formulation.

Table 2: Summary of IFS comparisons which isolate the effects of individual modifications to the convective parameterization

Convection Modification	IFS Comparison
Cy32r3 (ε_{org}^{RH} & τ)	OPER-CONV
ε_{org}^{RH} formulation	CAPE-CONV
τ	OPER-CAPE
ε_{org}^{RH} rate	OPER-ENTRN

2.2 Observational data

Daily outgoing longwave radiation (OLR) data is obtained from the National Oceanic and Atmospheric Administration (NOAA) Earth System Research Laboratory (ESRL). Readings from the Advanced Very High Resolution Radiometer (AVHRR) satellite are interpolated onto a global $2.5^\circ \times 2.5^\circ$ grid following Liebmann and Smith (1996). Comparisons are also made with ERA-Interim reanalysis data (Dee *et al.*, 2011) which is constructed using Cy31r1, as described in section 2.1.

2.3 Analysis technique

Many of the analysis techniques applied in this study are consistent with those of Waliser *et al.* (2009) as recognition of efforts in the modelling community to define a validation framework for assessing the simulation of the MJO. One such diagnostic is single-field wavenumber-frequency spectra for equatorially averaged (10°N - 10°S) OLR (section 3.3) and 850 hPa zonal wind (not shown). The spectra are calculated by applying a Fourier transformation to a 365-day timeseries (from May 2008 to April 2009) and forming power, resulting in a bandwidth of $(365)^{-1}$. By construction, positive wavenumbers and frequencies represent eastward propagation. For westward propagation to be identified, either the wavenumber or frequency must be negative. If there is equal power in the eastward and westward directions, then a standing oscillation is present.

A further diagnostic advocated by Waliser *et al.* (2009) and widely used to analyse MJO activity through the YOTC period is the real-time, multivariate MJO index (Wheeler and Hendon, 2004). The index is based on the first two combined empirical orthogonal functions (EOFs) of near-equatorially averaged OLR, and zonal winds at 850 hPa and 200 hPa, which together account for approximately 25% of the total variance. The positive and negative phases of EOF1 describe active and suppressed convection over the Maritime Continent region respectively. The positive (negative) phase of EOF2 describes active (suppressed) convection over the West Pacific and suppressed (active) convection over the Indian Ocean. The projection of the daily model data, with components of seasonal and interannual variability removed, onto the two combined EOFs produces two principal component Real-time Multivariate MJO (RMM) timeseries, RMM1 and RMM2. The indices effectively isolate MJO variability and, plotted in RMM phase space, indicate the propagation characteristics of individual events. The MJO amplitude is defined from the index as $\sqrt{RMM1^2 + RMM2^2}$. During April 2009 a strong MJO event is identified, this case study is analysed using the multivariate MJO index (section 3.4).

3 Results

3.1 Control IFS versions

The initial comparison between the control IFS versions, Cy31r1 and OPER, will indicate the progress in simulating MJO activity in the IFS since 2006. Intraseasonal OLR (Figure 1), 850 hPa zonal wind (Figure 2) anomalies are extracted using a 20-100 day bandpass filter. The integration period of the hindcast experiments is not long enough to apply the same filter. At a 1-day forecast lead time both Cy31r1 and OPER exhibit coherent eastward-propagating dynamical (Figure 2 (b) and (c)) and convective (Figure 1 (b) and (c)) signals on intraseasonal timescales, which agree well with observations.

At a 10-day forecast lead time the amplitude of the intraseasonal convective activity and the associated zonal wind anomalies in Cy31r1 have weakened considerably and the anomalies which do develop do

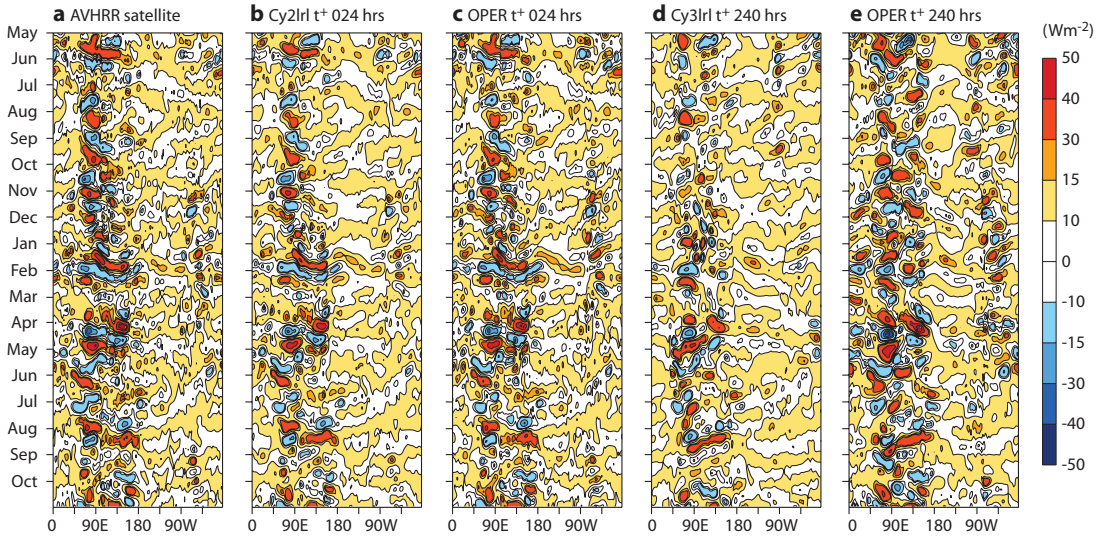

Figure 1: Hövmuller (time-longitude) diagrams of 20-100 day band-pass filtered OLR averaged between 10° N and 10° S. May 2008 to October 2009. (a) NOAA AVHRR satellite data. (b) and (d) Cy31r1 verified at 1- and 10-day forecast lead time, respectively. (c) and (e) OPER verified at 1- and 10-day forecast lead time, respectively.

not exhibit coherent eastward propagation (Figure 1 and 2 (d)). Conversely, in OPER increasing forecast lead time strengthens the convective anomalies, although they still exhibit a less coherent propagating structure compared with observations (Figure 1 (e)). At this lead time, OPER is particularly overactive in the Western Hemisphere; the convective anomalies which form between 60° W and 30° W are stronger than those observed by satellite. In OPER, the large-scale circulation pattern in the zonal wind is better preserved at a 10-day forecast lead time than the associated convective anomalies (Figure 2 (e)), this will be discussed further in section 4.1.

While this "old-model, new-model" comparison highlights improvements in the representation of the MJO, the model configurations differ considerably (Table 1), therefore, it cannot attribute those advances to specific model changes. It is only through comparisons with the hindcast experiments that the effect of individual model modifications can be extracted (Table 2).

3.2 Variance of convective activity

When considering the ability of a numerical weather model to simulate convective activity in the tropics, it is not sufficient to examine only the mean climate, but necessary to also examine the capability of the model to reproduce the correct variability about that mean. Figure 3 shows the unfiltered variance of convective activity in the tropics from AVHRR satellite data, the IFS control versions Cy31r1 and OPER, and the hindcast experiments CONV, ENTRN and CAPE, at a 1-day forecast lead time (Figure 3 (a)). The satellite data exhibits a similar spatial pattern in the variance of unfiltered OLR compared with the intraseasonally filtered equivalent (not shown). The largest variance of OLR is located over the equatorial Indian Ocean, Bay of Bengal, and West Pacific Warm Pool, extending south of the equator through the Australian monsoon region into the South Pacific convergence zone (SPCZ); there is little variance in daily OLR along the equatorial eastern Pacific. The larger Indonesian islands exhibit a local minimum in variance.

At a 1-day forecast lead time, all versions of the IFS reproduce the spatial pattern of variance in daily

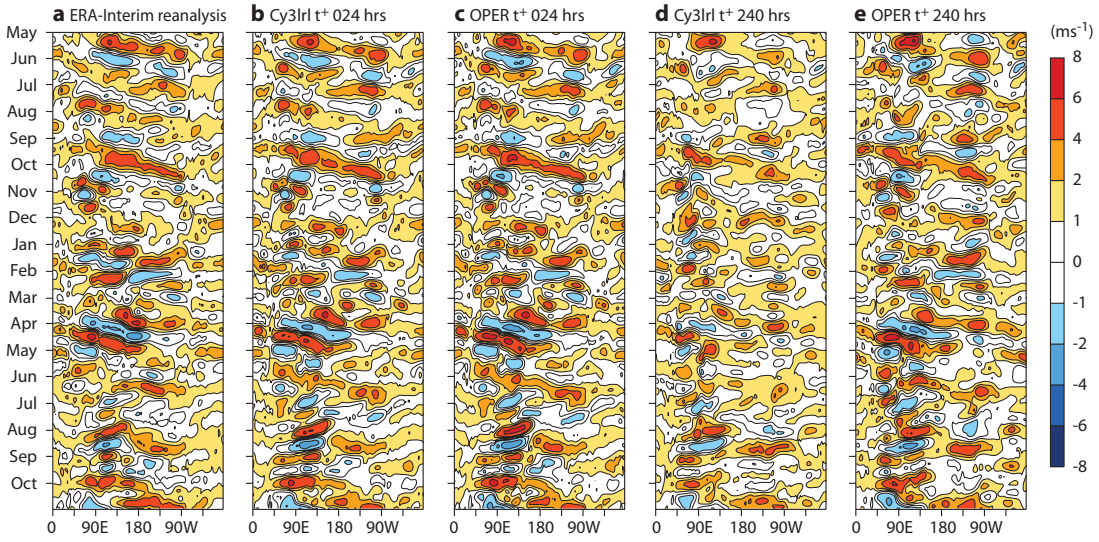

Figure 2: As Figure 1, but for 850 hPa zonal wind compared with, (a) ERA-Interim reanalysis.

OLR with reasonable accuracy. However, discrepancies are evident in the magnitude of convective variability. Comparing OPER and CONV (CAPE and CONV) with the satellite data indicates that the introduction of the Cy32r3 convection scheme (ε_{org}^{RH}) increased the magnitude of convective variability in the entire Indo-Pacific region (Figures 3 (a),(b),(d) and (f)). However, OPER overestimates the magnitude of convective variability in the South China and Philippine Seas, Australian monsoon region and SPCZ. CONV (Figure 3 (c)) shows slightly stronger variance than Cy31r1 (Figure 3 (b)), although both underestimate the magnitude of convective variability in the entire Indo-Pacific region. This suggests that the other, non-convection scheme changes between Cy31r1 and OPER, such as increased horizontal and vertical resolution, and the introduction of McRad, the new radiation scheme, had little effect on the simulation of convective activity in the tropics (Figures 3 (a)-(c)). Comparing CAPE and OPER suggests that a possible effect of reverting to a constant CAPE adjustment timescale (τ) is that the representation of the minimum in convective activity over the Indonesian islands is slightly improved. However, compared with observations, there is still too much variability over the islands (Figures. 3 (a),(d) and (f)). Halving the rate of ε_{org}^{RH}, or reducing total entrainment by approximately 25%, has little impact on the variability of convective activity- the overestimations in OPER are slightly amplified in ENTRN (Figures 3 (a),(d) and (e)).

As forecast lead time increases, all versions of the IFS exhibit an increase in convective activity. The largest of which is a significant overestimation of convective activity in the northern Indian Ocean and Australian monsoon region compared with observations resulting from the ε_{org}^{RH} formulation (not shown). Therefore, Figure 3 shows that a dominant impact of the modified Cy32r3 convection scheme, more specifically ε_{org}^{RH}, is to increase the variability of convective activity in the Indo-Pacific region.

3.3 Space-time power spectrum

Single-field wavenumber-frequency spectra (section 2.3) are calculated for all the versions of the IFS and compared with observations. The satellite-derived AVHRR OLR (Figure 4) exhibit a concentration of power at 20-80 day periods and eastward-propagating zonal wavenumber 1-3, consistent with the intraseasonal frequency and propagation characteristics of the MJO. At 20-80 day periods the eastward

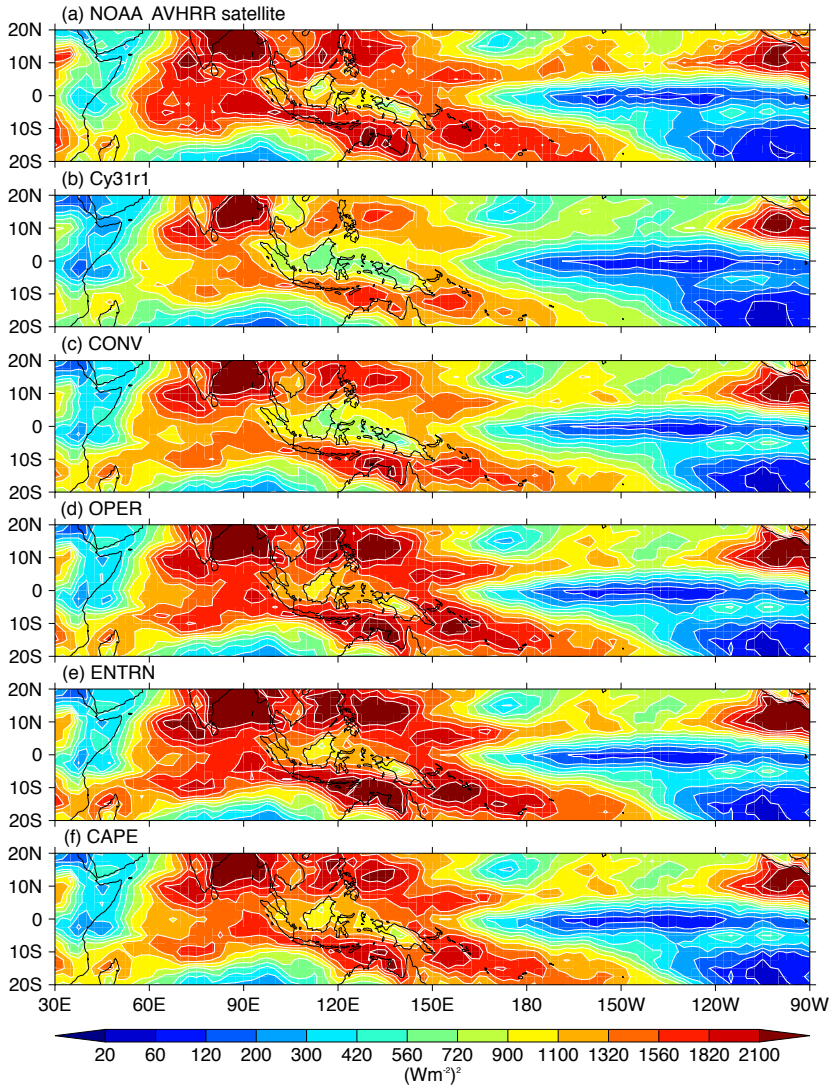

Figure 3: Variance of unfiltered OLR for May 2008 to April 2009 from (a) NOAA AVHRR satellite data and Cy31r1, CONV, OPER, ENTRN and CAPE (b)-(f) at 1-day forecast lead time.

power in OLR is approximately 5 times the westward power. Both eastward and westward power are evident at higher frequencies in the OLR, indicating the existence of standing oscillations and lower-frequency propagating features. At a 1-day forecast lead time, all versions of the IFS exhibit a concentration of power at 20-80 day periods and zonal wavenumber 1, although the modelled power is weaker than observed.

At a 5-day forecast lead time there is a consistent overestimation, compared with observations, of power in low-frequency westward- and eastward-propagating wavenumbers. The impact of the Cy32r3 convection scheme at a 5-day forecast lead time (Figure 4 (f) and (j)) is to increase the power in low-frequency eastward-propagating wavenumbers, and slightly increase the power in the MJO signal and intraseasonal westward-propagating wavenumbers. ε_{org}^{RH} is responsible for these changes (Figure 4 (f) and (n)) but, the variable τ has little effect (Figure 4 (i) and (n)). The simulation of MJO power is not sensitive to the rate of ε_{org}^{RH} (Figure 4 (i) and (l)). At a 10-day forecast lead time, models with the pre-Cy32r3 convection scheme (Cy31r1 and CONV) exhibit a distinct weakening of the power in the intraseasonal frequencies

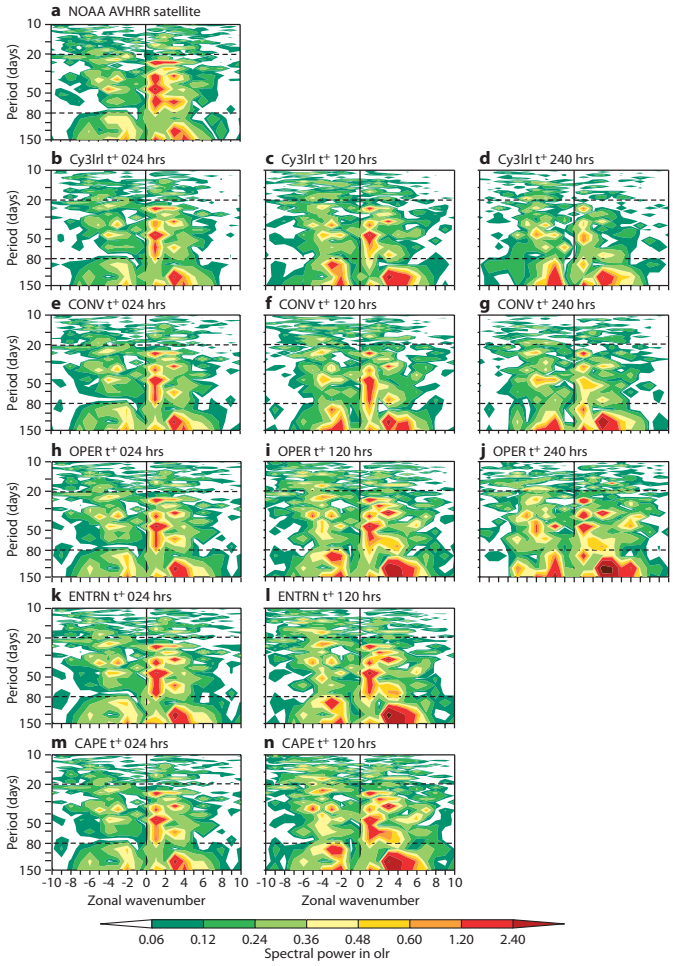

Figure 4: Space-time power spectra in equatorially averaged (10°N - 10°S) OLR for (a) NOAA AVHRR satellite data, (b)-(j) Cy31r1, CONV and OPER at 1-, 5- and 10-day forecast lead time, (k)-(n) ENTRN and CAPE at 1- and 5-day forecast lead time. Eastward and westward propagation are represented by the right and left hand side of the diagrams, respectively. Horizontal dashed lines have been added at 20 and 80 days to highlight the typical period of the MJO.

associated with the MJO. The Cy32r3 convection scheme (OPER) is able to maintain the power of the eastward-propagating intraseasonal frequencies at a 10-day forecast lead time, although the power of the westward-propagating intraseasonal frequencies also increases, and is stronger than observed (Figure 4 (d),(g) and (j)). Results are similar for 850 hPa zonal wind (not shown). Therefore, using space-time power spectrum analysis it has been shown that ε_{org}^{RH} in the Cy32r3 convection scheme is responsible for maintaining the eastward-propagating intraseasonal power signal in OLR (Figure 4) and 850 hPa wind (not shown) associated with the MJO at longer forecast lead times.

3.4 Multivariate MJO index

The multivariate MJO index (section 2.3) is used to evaluate the overall skill of the IFS in predicting the onset and evolution of the MJO. Linear correlations are performed between the timeseries of observed EOF1 and EOF2 and those produced from the IFS at each forecast lead time. A forecast is typically considered as skilful if the correlation exceeds 0.6 (e.g. Vitart and Molteni, 2010), therefore, this threshold

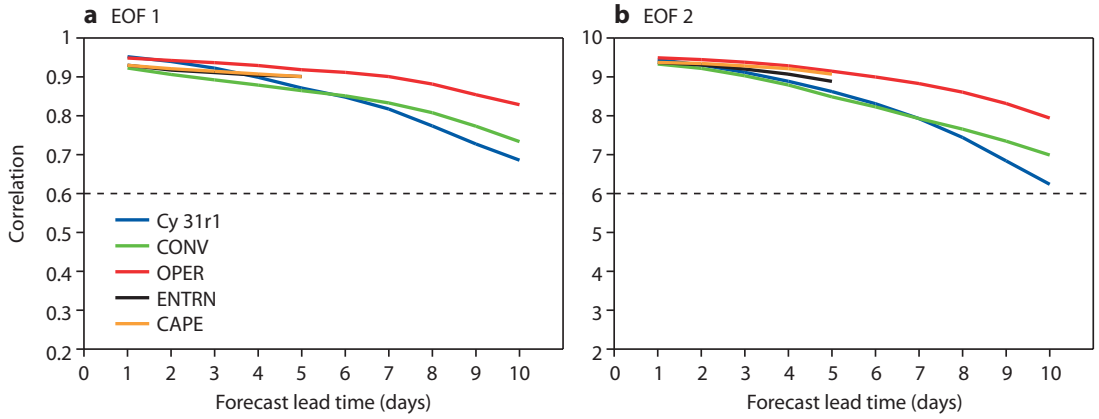

Figure 5: Linear correlations between observed and forecast (a) EOF1, (b) EOF2, (c) MJO amplitude and (d) MJO amplitude ≥ 1 as a function of forecast lead time for the period from May 2008 to April 2009. The CAPE and ENTRN hindcast experiments do not extent to a 10-day forecast lead time.

has been included in the diagrams.

According to Figures. 5 (a) and (b), at a 5-day forecast lead time, ENTRN and CAPE exhibit similar levels of skill as OPER in predicting EOF1 and EOF2. Cy31r1, CONV and OPER all have skill (correlation > 0.6) in predicting EOF1 and EOF2 at a 10-day forecast lead time. At the longer lead times, the IFS exhibits more skill in predicting EOF1, when the enhanced convective anomaly enters the Maritime Continent, than EOF2, when the enhanced convective anomaly is in the central Pacific. This is consistent with previous studies which have shown that the IFS has difficulty propagating the enhanced convection associated with the MJO through the Maritime Continent (e.g. Inness and Slingo, 2006; Vitart and Molteni, 2010). Although slight improvements in skill are apparent between Cy31r1 and CONV at longer forecast lead times, comparing CONV and OPER shows that large improvements in skill can be directly attributed to the Cy32r3 convection scheme. Skilful prediction of the MJO amplitude (MJO amplitude ≥ 1) is increased by four (two) days with the introduction of the Cy32r3 convection scheme (Figure 5).

The diagnostics shown so far have described MJO activity through the YOTC period. One advantage of using an NWP approach to analysing MJO simulation is that individual MJO case studies can be analysed and compared with observations. The multivariate MJO index is used to analyse the April 2009 case study (Figure 6). The strong amplitude and eastward propagation are clear in both the observations (black line) and ERA-Interim reanalysis (dark red line). At the start of April, as the enhanced convection associated with the MJO entered the Indian Ocean, it already had a large amplitude. The amplitude remained large as, during April, the MJO signal propagated across the Indian Ocean, through the Maritime Continent and into the West Pacific. As forecast lead time increases, there is a distinct loss of MJO amplitude in the pre-Cy32r3 convection scheme cycles of the IFS (Cy31r1, CONV; Figures 6 (a) and (b)). At longer forecast lead times, the effect of ε_{org}^{RH} (comparing CONV with CAPE) is to increase the amplitude of the MJO. The most prominent increase in MJO amplitude is in the Indian Ocean, resulting in a large overestimation compared with observations. The increase in MJO amplitude results in an underestimation of MJO activity which is relatively small in the Maritime Continent but much larger in the West Pacific. The main effect of the variable τ (comparing CAPE with OPER) is to reduce the amplitude of the MJO in the Indian Ocean; there is little impact in other regions. The compensating effects of ε_{org}^{RH} and τ which increase and decrease the amplitude of the MJO in the Indian Ocean respectively, mean that at longer forecast lead times, the Cy32r3 convection scheme (comparing CONV with OPER) maintains

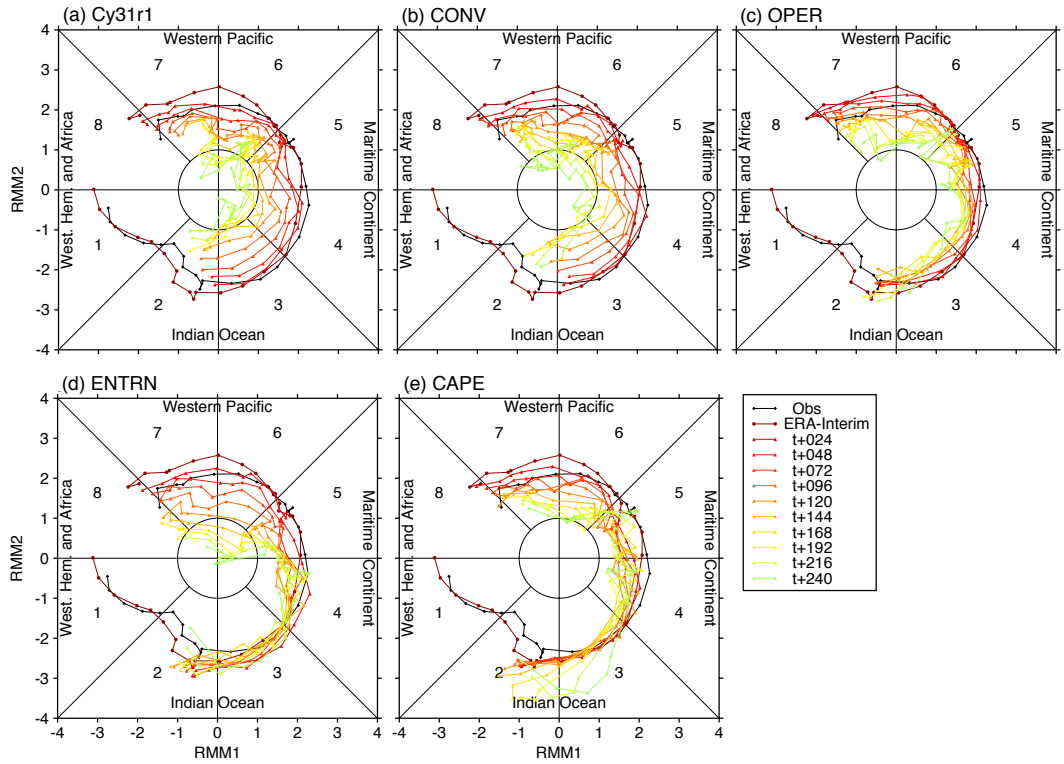

Figure 6: Multivariate MJO index for the April 2009 case study from observations (black line), ERA-Interim reanalysis (dark red line) and versions of the IFS plotted on forecast validation date at increasing forecast lead time from 1-day (red line) to 5-days (light orange line). Observations refer to RMM1 and RMM2 calculated using satellite-derived OLR and NCEP reanalysis zonal winds at 850 hPa and 200 hPa.

the observed magnitude of MJO amplitude in that region. However, at longer forecast lead times, in the Maritime Continent and especially in the West Pacific, the Cy32r3 convection scheme exhibits less skill than in the Indian Ocean in predicting the evolution of the April 2009 MJO.

4 Discussion of Results

4.1 Convective versus dynamical signal of the MJO

The comparison between the control versions of the IFS (section 3.1) suggests that, at short forecast lead times, both Cy31r1 and OPER are able to reproduce anomalous, eastward-propagating signals in the OLR and zonal wind associated with the MJO. At a 10-day forecast lead time, however, OPER consistently maintains the intraseasonal MJO signal better than Cy31r1. The large-scale dynamical signal of the MJO (Figure 2) is better preserved at a 10-day forecast lead time in OPER than the associated convective signal (Figure 1). The convective and large-scale circulation signals associated with the MJO are widely considered to be strongly coupled; however, this result implies that there is a lack of coherence between the convective heating and the large-scale wave forcing in the IFS as forecast lead time increases. This characteristic of the IFS prompts the question of whether the model is producing an MJO-like signal for the wrong reasons. Interestingly, this is not a feature exclusive to the IFS, but is consistent with other studies. Comparing four pairs of coupled and uncoupled global simulations, Zhang *et al.* (2006) showed that the precipitation signal associated with the MJO was much weaker than observed, while the

dynamical signal in the zonal winds was stronger than observed, a characteristic common among many global circulation models (Kim *et al.*, 2009).

4.2 Reduction of eastward-propagating spectral power

The advances in MJO simulation can be summarised using a metric derived from the wavenumber-frequency spectra discussed in section 3.3. Figure 7 shows the east-west ratio of MJO spectral power, defined as the 20-80 day mode within wavenumbers 1-3 for OLR and 1-2 for 850 hPa zonal wind. In observations (AVHRR OLR and ERA-Interim 850 hPa zonal wind), the east-west power is 3-4 for OLR and 4-5 for zonal wind. Since the forecasts are initiated from ERA reanalysis, unsurprisingly all versions of the IFS exhibit equivalent east-west ratios of zonal wind to ERA-Interim (4-5). The forecast east-west ratios of OLR, however, are significantly reduced (2-3) compared with observations (3-4). As forecast lead time increases, versions of the IFS with ε_{org}^{RH} (OPER, CAPE and ENTRN; red, orange and black lines) maintain a higher east-west ratio than those with ε_{org}^{MC} (Cy31r1 and CONV; blue and green lines), which are reduced significantly by a 10-day forecast lead time. Therefore, Figure 7 shows that, with the modified formulation of organised entrainment, the IFS is able to maintain the eastward-propagating spectral power of the MJO at longer forecast lead times. Using a similar metric, studies have shown that a smaller-than- observed east-west ratio of MJO spectral power is a common feature among most of the CMIP3 models (Lin *et al.*, 2006) and state-of-the-art climate models (Kim *et al.*, 2009).

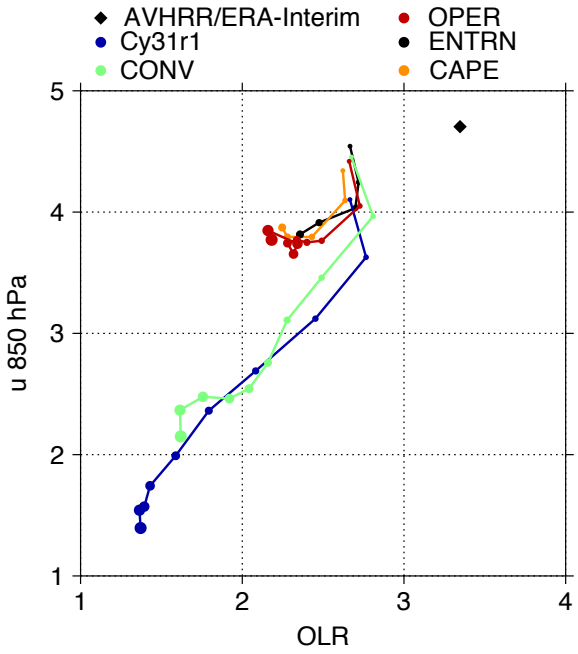

Figure 7: East-west ratio of MJO (20-80 day mode, within wavenumbers 1-3 for OLR and 1-2 for zonal wind) spectral power calculated by dividing the sum of eastward-propagating power by the westward-propagating equivalent. The ratio from AVHRR OLR and ERA-Interim 850 hPa zonal wind (black diamond) is is compared to all of the versions of the IFS described in Table 1. Lines (and increasing dot size) refer to increasing forecast lead time up to 5 days for CAPE and ENTRN (orange and black lines) and 10 days for Cy31r1, CONV and CAPE (blue, green and red lines).

5 Conclusions

The hindcast experiments performed in this study present a unique opportunity to attribute changes in the simulation of the MJO in the IFS seen in B08 to individual model modifications. MJO diagnostics (Waliser *et al.*, 2009) have been applied to the versions of the IFS described in Table 1. Although both Cy31r1 and OPER are able to reproduce the eastward-propagating, intraseasonal signal of the MJO at a 1-day forecast lead time (Figures 1 and 2), Cy31r1 underestimates the variance in convective activity across the equatorial Indo-Pacific region. OPER is able to reproduce the observed variance of convective activity on the intraseasonal timescales of the MJO after a 1- day forecast lead time (Figure 3) but, because variance increases with increasing lead time, OPER significantly overestimates the convective variance later in the forecast. Through comparison with the hindcast experiments, it was shown that the Cy32r3 convective parameterization alone increased the predictive skill of the EOFs during the YOTC period by 3 days (Figure 5). Additionally, the Cy32r3 formulation of convection, or ε_{org}^{RH} specifically, increased the variability of convective activity across the entire equatorial Indian Ocean and West Pacific Warm Pool (Figure 3). The simulation of convective variability is shown to be more sensitive to the formulation of entrainment than the rate of entrainment, while changing to a variable CAPE timescale in the closure for deep convection had little effect. Therefore, the introduction of the Cy32r3 convective parameterization has led to an overactive MJO in the IFS; cycle 35r3 implemented in October 2009 has been shown to partially solve this problem (Vitart and Molteni, 2010).

An advantage of the NWP approach to studying the MJO is that the specific characteristics of individual events, in this case the April 2009 MJO, can be examined in model simulations and direct comparisons can be made with observational data. Consistent with the increased convective activity, ε_{org}^{RH} increased the amplitude of the MJO in all regions. The new variable CAPE adjustment timescale reduced the amplitude of the MJO in the Indian Ocean. Therefore, the combined impact of the Cy32r3 convective parameterization was to maintain the amplitude of the MJO at longer forecast lead times. Again, the simulation of the MJO was shown to be more sensitive to the formulation of entrainment than the entrainment rate (Figure 6).

This study has shown that improvements in the simulation of the MJO in the IFS can be directly attributed to the formulation of convection in Cy32r3, specifically, the relative-humidity-dependent formulation for organised entrainment. The decision to move to a formulation for entrainment that was dependent on relative humidity was motivated by the recognition that environmental moisture is crucial in modulating the location and strength of convective activity on MJO timescales (Redelsperger *et al.*, 2002; Grabowski, 2003; Grabowski and Moncrieff, 2004). However, it is not just the humidity dependence of the organised deep entrainment rate which is important to the accurate simulation of cumulus convection in the IFS. de Rooy *et al.* (2012) conclude that, although the relative-humidity-dependent entrainment factor in the IFS is very important, it is more important that the overall entrainment constant is large. Therefore, the sensitivity to the environmental moisture in the IFS can be thought of as twofold; having strong entrainment at cloud base provides the 'first' sensitivity to the environment, while having a relative-humidity-dependent formulation for organised entrainment during the parcel ascent the 'second'.

While the diagnostics applied in this study, and metrics such as that in Figure 7, can highlight deficiencies in the ability of numerical models to simulate the MJO, they cannot alone provide insight into the physical mechanisms responsible. For example, with these diagnostics alone, the MJO can be fully characterised in a model but conclusions cannot be drawn about which processes are integral to its onset and evolution. This has led to the recognition that more process-based diagnostics should be applied to simulations of the MJO (e.g. Zhu *et al.*, 2009; Kim *et al.*, 2009). The discussion and application of such diagnostics and this mechanistic approach will be the subject of Hirons *et al.* (2012).

Acknowledgements

The author would like to thank the National Environmental Research Council (NERC) for providing the PhD scholarship that made this work possible and ECMWF for their support of this work.

References

Bechtold P, Köhler M, Jung T, Doblas-Reyes F, Leutbecher M, Rodwell MJ, Vitart F, Balsamo G. 2008. Advances in simulating atmospheric variability with the ECMWF model: From synoptic to decadal time-scales. *Q. J. R. Meteorol. Soc.* **134**: 1337–1351.

Bond NA, Vecchi GA. 2003. The Influence of the Madden-Julian Oscillation on Precipitaion in Oregon and Washington. *Weather Forecasting* **18**: 600–613.

de Rooy WC, Bechtold P, Frölich K, Hohenegger C, Jonker H, Mironov D, Siebesma AP, Teixeira J, Yano JI. 2012. Entrainment and detrainment in cumulus convection: an overview. *Q. J. R. Meteorol. Soc.* .

Dee DP, Uppala SM, Simmons AJ, Berrisford P, Poli P, Kobayashi S, Andrae U, Balmaseda MA, Balsamo G, Bauer P, Bechtold P, Beljaars ACM, van de Berg L, Bidlot J, Bormann N, Delsol C, Dragani R, Fuentes M, Geer AJ, Haimberger L, Healy SB, Hersbach H, Holm EV, Isaksen L, Kallberg P, Kohler M, Matricardi M, McNally AP, Monge-Sanz BM, Morcrette JJ, Park BK, Peuby C, de Rosnay P, Tavolato C, Thepaut JN, Vitart F. 2011. The ERA-Interim reanalysis: configuration and performance of the data assimilation system. *Q. J. R. Meteorol. Soc.* **137**: 553–597.

Derbyshire SH, Beau I, Bechtold P, Grandpeix JY, Piriou JM, Redelsperger JL, Soares PMM. 2004. Sensitivity of moist convection to environmental humidity. *Q. J. R. Meteorol. Soc.* **130**: 3055–3079.

Grabowski WW. 2003. MJO-like Coherent Structures: Sensitivity Simulations using the Cloud-Resolving Convection Parameterization (CRCP). *J. Atmos. Sci.* **60**: 847–864.

Grabowski WW, Moncrieff MW. 2004. Moisture-convection feedback in the tropics. *Q. J. R. Meteorol. Soc.* **130**: 3081–3104.

Hendon HH, Liebmann B. 1990. The Intraseasonal (30-50 day) Oscillation of the Australian Summer Monsoon. *J. Atmos. Sci.* **47**: 2909–2923.

Hirons LC, Inness P, Vitart F. 2012. Understanding advances in the simulation of intraseasonal variability in the ECMWF model. Part II: The application of process-based diagnostics. *Q. J. R. Meteorol. Soc.* .

Inness PM, Slingo JM. 2006. The Interaction of the Madden-Julian Oscilltion with the Maritime Continent in a GCM. *Q. J. R. Meteorol. Soc.* **132**: 1645–1667.

Kessler WS, McPhaden MJ. 1995. Forcing of intraseasonal Kelvin waves in the equatorial Pacific. *J. Geophys. Res* **100**: 10,613–10,631.

Kim D, K, Stern W, Waliser D, Kang IS, Maloney ED, Wang W, Weickmann K, J Benedict MK, Lee MI, Neale R, Suarez M, Thayer-Calder K, Zhang G. 2009. Application of MJO Simulation Diagnostics to Climate Models. *J. Climate.* **22**: 6413–6436.

Lawrence DM, Webster PJ. 2002. The Boreal Summer Intraseasonal Oscillation: Relationship between Northward and Eastward Movement of Convection. *J. Atmos. Sci.* **59**: 1593–1606.

Liebmann B, Smith CA. 1996. Description of a complete (interpolated) OLR dataset. *Bull. Amer. Meteor. Soc* **77**: 1275–1277.

Lin JL, Kiladis GN, Mapes BE, Weickmann KM, Sperber KR, Lin W, Wheeler MC, Schubert SD, Genio AD, Donner LJ, Emori S, Gueremy JF, Hourdin F, Rasch PJ, Roeckner E, Scinocca JF. 2006. Tropical Intraseasonal Variability in 14 IPCC AR4 Climate Models. Part I: Convective Signals. *J. Climate.* **19**: 2665–2690.

Madden RA, Julian PR. 1971. Detection of a 40-50 Day Oscillation in the Zonal Wind in the Tropical Pacific. *J. Atmos. Sci.* **28**: 702–708.

Maloney ED, Hartmann DL. 2000. Modulation of Eastern North Pacific Hurricanes by the Madden-Julian Oscillation. *J. Climate.* **13**: 1451–1460.

Matthews AJ. 2004. Intraseasonal Variability over Tropical Africa during Northern Summer. *J. Climate.* **17**: 2427–2440.

Mo KC. 2000. Intraseasonal Modulation of Summer Precipitation over North America. *Mon. Wea. Rev.* **128**: 1490–1505.

Morcrette JJ, Barker HW, Iacono MJ, Mozdzynski G, Pincus R, Salmond D, Serrar S. 2007. A new radiation package McRAD. *ECMWF Newsletter* **112**: 22–32.

Nakazawa T. 1988. Tropical Super Clusters within Intraseasonal Variations over the Western Pacific. *J. Met. Soc. Japan* **66**(6): 823–839.

Redelsperger JL, Parsons DB, Guichard F. 2002. Recovery processes and factors limiting cloud-top height following the arrival of a dry intrusion observed during TOGA-COARE. *J. Atmos. Sci.* **59**: 2438–2457.

Salby ML, Garcia RR, Hendon HH. 1994. Planetary-Scale Circulations in the Presence of Climatological and Wave-Induced Heating. *J. Atmos. Sci.* **51**(16): 2344–2367.

Slingo JM, Sperber KR, Boyle JS, Ceron JP, Dix M, Dugas B, Ebisuzaki W, Fyfe J, Gregory D, Gueremy JF, Hack J, Harzallah A, Inness P, Kitoh A, Lau WKM, McAvaney B, Madden RA, Matthews AJ, Palmer TN, Park CK, Randall DA, Renno N. 1996. Intraseasonal oscillations in 15 atmospheric general circulation models: results from an AMIP diagnostic subproject. *Climate Dynamics* **12**: 325–357.

Vitart F. 2003. Monthly forecasting system. Technical Report 424, ECMWF.

Vitart F, Molteni F. 2010. Simulation of the MJO and its teleconnections in the ECMWF forecast system. *Q. J. R. Meteorol. Soc.* **136**: 842–855.

Vitart F, Woolnough SJ, Balmaseda MA, Tompkins AM. 2007. Monthly Forecast of the Madden-Julian Oscillation using a Coupled GCM. *Mon. Wea. Rev.* **135**: 2700–2715.

Waliser DE, Sperber KR, Hendon HH, Kim D, Maloney ED, Wheeler MC, Weickmann KM, Zhang C, Donner L, Gottschalck J, Higgins W, Kang IS, Legler D, Moncrieff M, Schubert S, Stern W, Vitart F, Wang B, Wang W, Woolnough SJ. 2009. MJO Simulation Diagnostics. *J. Climate.* **22**: 3006–3030.

Wheeler MC, Hendon HH. 2004. An All-Seasonal Real-Time Multivariate MJO Index: Development of an Index for Monitoring and Prediction. *Mon. Wea. Rev.* **132**: 1917–1932.

Woolnough SJ, Vitart F, Balmaseda MA. 2007. The role of the ocean in the Madden-Julian Oscillation: Implications for MJO prediction. *Q. J. R. Meteorol. Soc.* **133**: 117–128.

Zhang C. 2005. Madden-Julian Oscillation. *Rev. Geophys.* **43**: RG2003, doi:10.1029/2004RG000158.

Zhang C, Dong M, Gualdi S, Hendon HH, Maloney ED, Marshall A, Sperber KR, Wang W. 2006. Simulations of the Madden-Julian Oscillation in four paris of coupled and uncoupled global models. *Climate Dynamics* **27**: 573–592.

Zhu H, Hendon HH, Jakob C. 2009. Convection in a Parameterized and Superparameterized Model and Its Role in the Representation of the MJO. *J. Atmos. Sci.* **66**: 2796–2811.